Channel Selection for Gesture Recognition Using Force Myography: A Universal Model for Gesture Measurement Points

Ziyu Xiao, Zihao Du, Zefeng Yan, Tiantian Huang, Denan Xu, *Member, IEEE*, Qin Huang, and Bin Han, *Member, IEEE*

***Abstract*— Gesture recognition has emerged as a significant research domain in computer vision and human-computer interaction. One of the key challenges in gesture recognition is how to select the most useful channels that can effectively represent gesture movements. In this study, we have developed a channel selection algorithm that determines the number and placement of sensors that are critical to gesture classification. To validate this algorithm, we constructed a Force Myography (FMG)-based signal acquisition system. The algorithm considers each sensor as a distinct channel, with the most effective channel combinations and recognition accuracy determined through assessing the correlation between each channel and the target gesture, as well as the redundant correlation between different channels. The database was created by collecting experimental data from 10 healthy individuals who wore 16 sensors to perform 13 unique hand gestures. The results indicate that the average number of channels across the 10 participants was 3, corresponding to an 75% decrease in the initial channel count, with an average recognition accuracy of 94.46%. This outperforms four widely adopted feature selection algorithms, including Relief-F, mRMR, CFS, and ILFS. Moreover, we have established a universal model for the position of gesture measurement points and verified it with an additional five participants, resulting in an average recognition accuracy of 96.3%. This study provides a sound basis for identifying the optimal and minimum number and location of channels on the forearm and designing specialized arm rings with unique shapes.**

***Index Terms*— Gesture recognition, channel selection, force myography (FMG), sensor placement, recognition accuracy.**

Manuscript received 30 November 2023; revised 17 April 2024; accepted 13 May 2024. Date of publication 21 May 2024; date of current version 29 May 2024. This work was supported in part by the Natural Science Foundation of Hubei Province of China under Grant 2022CFB239, in part by the National Natural Science Foundation of China under Grant 52375015, in part by the Guangdong Basic and Applied Basic Research Foundation under Grant 2021A1515011717, and in part by the Interdiciplinary Research Program of Huazhong University of Science and Technology (HUST) under Grant 2023JCYJ013. *(Corresponding author: Bin Han.)*

This work involved human subjects or animals in its research. Approval of all ethical and experimental procedures and protocols was granted by the Ethics Committee of the Huazhong University of Science and Technology, and performed in line with the Declaration of Helsinki.

Ziyu Xiao, Zefeng Yan, Tiantian Huang, and Bin Han are with the State Key Laboratory of Intelligent Manufacturing Equipment and Technology, School of Mechanical Science and Engineering, Huazhong University of Science and Technology, Wuhan 430074, China (e-mail: zyxiao@hust.edu.cn; Zfyan@hust.edu.cn; huangtt110@hust.edu.cn; binhan@hust.edu.cn).

Zihao Du is with the Department of Automation, School of Information Science and Technology, Tsinghua University, Beijing 100084, China (e-mail: zihaodu@mail.tsinghua.edu.cn).

Denan Xu is with Guangdong Intelligent Research Institute, Dongguan 523808, China (e-mail: denanxu@hust.edu.cn).

Qin Huang is with the Department of Rehabilitation Medicine, Union Hospital, Tongji Medical College, Huazhong University of Science and Technology, Wuhan 430030, China (e-mail: judy1130@126.com).

This article has supplementary downloadable material available at https://doi.org/10.1109/TNSRE.2024.3403941, provided by the authors.

Digital Object Identifier 10.1109/TNSRE.2024.3403941

I. Introduction

UPPER limb amputation often results in both severe physical dysfunction and psychological imbalance to patients [1], [2]. Intent recognition is the capability of machines to accurately interpret human intent. The integration of advanced intention recognition methods with active prosthetics and the real-time control of prosthetics through a Human-Machine Interface (HMI) can enable patients to effortlessly perform a variety of functions in diverse environments [3], [4]. Through the indirect monitoring of forearm muscle activities associated with hand movements, gesture recognition can be captured effectively and conveniently. Prominent methodologies for this purpose include gaze tracking [5], [6], Surface Electromyography (SEMG) [7], [8], [9], Electroencephalography (EEG) [10], and Mechanomyography (MMG) [11]. SEMG, in particular, records the electrophysiological activities of muscle tissues, offering a direct reflection of the real-time neural and muscular status during movement. This has led to its extensive application in prosthetic control and neurorehabilitation engineering [12]. However, SEMG faces several unresolved challenges, such as low signal strength (in microvolts), inferior sensor signal quality, susceptibility to crosstalk from other biopotentials, significant system power consumption, and the complexity of signal interpretation. Moreover, SEMG-based systems typically depend on electrodes that must be precisely positioned; these electrodes are susceptible to electromagnetic interference and other noises and are sensitive to various physiological conditions, including skin resistance, perspiration, body hair, and fatigue [13]. Contrasting with techniques that measure bioelectrical activities, there exists a category focused on

the measurement of mechanical activities in muscles [14]. For example, MMG leverages microphones, accelerometers, or laser displacement sensors to capture the mechanical vibrations or acoustic signals of muscles, facilitating the detection of muscle contractions and relaxations [15]. MMG is particularly advantageous for assessing muscle fatigue and quality, exhibiting lower sensitivity to changes in skin surface conditions such as sweating.

Force Myography (FMG) is a technology for gesture control that operates through the detection of changes in muscle hardness or volume [16], [17], [18]. As muscles engage in activities, such as contraction, their volume and shape undergo alterations. These changes are detectable by deploying pressure sensors, strain gauges, or other devices capable of sensing muscle deformation on the muscle surface. The signals generated from these sensors are utilized to identify specific muscle activities or gestures. The advantages of FMG are primarily highlighted in the following areas:

1) High signal-to-noise ratio and strong anti-interference capability [14];
2) Cost-Effectiveness with comparable recognition accuracy [19];
3) Ease of use and superior performance in dynamic motions [20];
4) Low sampling frequency and simplified signal processing [21].

Over the past two decades, researchers have developed a variety of methods for upper limb movement prediction and finger angle estimation using FMG [22], [23]. Many scientific studies have shown that FMG has been proven to be a safe, stable, reliable, and non-invasive active prosthetic control interface [24], [25].

The muscles and nerves of the human upper limb are complex and have many degrees of freedom. Due to the specific muscle pressure targeted by the FMG technology, the placement of the FSR sensor has a significant impact on the accuracy of the motion classification [26]. A study of upper limb movements showed that increasing the spatial coverage location of FSR sensors significantly improves accuracy and that different combinations of FSR arm bands produced different results [27]. A study on the minimum number of channels for gesture recognition showed that using eight sensors can achieve good gesture classification, and that optimizing the sensor layout can significantly improve the classification accuracy [28]. Despite its relatively low cost, the complexity of the FMG system increases as the number of sensors used increases. This leads to an increase in storage space and computational overhead required for the growing sample data, along with a overflow of redundant features. Feature selection is a technique that reduces the number of irrelevant features without sacrificing prediction accuracy [29], [30]. In this research, we examine the possibility of treating each sensor as a feature and apply feature selection methods to eliminate channels that are less relevant. This approach reduces the number of sensors and computational overhead, leading to improved classification accuracy.

Chakaveh Ahmadizadeh et al. [31] evaluated five commonly used feature selection methods, including Sequential Forward Selection (SFS) with two different stopping criteria, Minimum Redundancy-Maximum Relevance (mRMR), Genetic Algorithm (GA), and Boruta. The results showed that three of the five methods were able to significantly reduce the number of channels while maintaining decent classification accuracy of all datasets, demonstrating the feasibility of dimensionality reduction using feature selection methods. Wang et al. [32] studied the optimization of sEMG channels using a genetic algorithm. Six healthy participants performed 13 gestures, and the results showed that using 11 electrodes achieved a 97% accuracy rate in gesture recognition, and placing the electrodes in the middle of the forearm resulted in better performance than placing them at the front of the forearm. Although feature selection algorithms have been proven to be applicable in dimensionality reduction for gesture recognition systems, there are still some important shortcomings:

1) ignoring sensor distribution, sensor weight coefficient allocation and redundancy.
2) converging too quickly, easily falling into local optima.
3) insufficient richness of candidate subsets.

While FMG technology holds potential for gesture classification, the precise placement and quantity of sensors on the upper limb have not been extensively explored. Therefore, an algorithm for directly determining optimal sensor quantity and placement is crucial for gesture classification. Additionally, investigating the general sensor quantity and arrangement on the upper limb is significant. Unlike prior studies that reduce dimensionality post-data extraction, our novel approach treats each sensor as an individual feature and proposes a sensor grouping-based feature selection method.

This study employed a three-arm circular device equipped with a total of 16 sensors, which focused on exploring the essential 13 gestures in daily life. Our proposed feature selection method is compared with the well-known Relief-F, ILFS, CFS, and mRMR methods, and the results showed that our method has superior performance. The results from a further experiment demonstrated that even for the experiment participants who were not pre-trained, using only the recommended four measurement points to train the 13 gestures could still achieve a testing accuracy of over 90%. In conclusion, the findings of this study can not only help users to collect data from high-density FMG systems and determine the optimal number and location of sensors that contribute the most to gesture recognition, thereby enabling personalized device design, but also propose the general number and location of measurement points that provide a foundation for the next generation of universal and simplified technology devices.

II. The Optimal Channel Selection Algorithm

The developed channel (feature) selection algorithm is divided into three parts, schematically shown in Fig. 2 and the pseudo code is shown in Fig. 3.

A. Ranking of Channel Importance

We calculate the correlation between channels to rank the importance of each one, thereby discovering the best

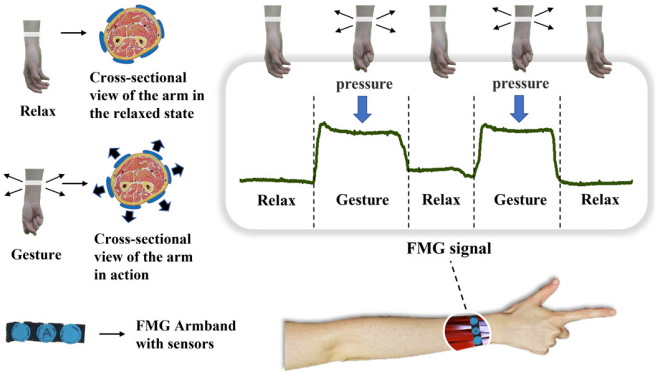

Fig. 1. Individual FMG sensor signals during gesture recognition.

combination of channels. Consider a set of M object classes $\{O_1, \ldots, O_m\}$, L channels, and Q armbands. In the context of FMG, let $x_t \in \hat{E}R_t$ denote the observable state of the muscle, which reflects the mechanical deformation of the skin and underlying tissues due to the contraction of the muscle fibers. Each participant's measurement generates a labeled FMG signal training dataset φ:

$$\varphi = \{(x_1, y_1), \ldots, (x_1, y_N), \ldots, (x_L, y_N)\} \tag{1}$$

where column N is the product of the measurement time t and the sampling frequency f, reflecting the number of columns in the raw data. Each action is measured twice for each participant to reduce measurement noise and variability.

The data $\varphi_{L\times N}$ from L sensors capturing the same action are concatenated into a matrix $\emptyset_{(2\times L\times M)\times N}$, which contains all the raw data for a participant's set of actions. This matrix, which can be quite large, may be subjected to various preprocessing steps, such as filtering and artifact removal, to improve the quality of the signals. Once the preprocessing is complete, each column of the matrix corresponds to a channel, resulting in the matrix $D = \tilde{\emptyset}_{n\times 1} = \{X, Y\}$. The rows of this matrix represent the measurements taken over time, while the columns correspond to L different channels, each of which is associated with a specific muscle group. To improve the convergence speed and accuracy of the subsequent model, the matrix D is standardized using min-max normalization. The transformation function is defined as follows:

$$x_{new} = \frac{x - x_{\min}}{x_{\max} - x_{\min}} \tag{2}$$

Let the weight matrix of the channels be $W = (0, \ldots, 0)_L$, and the weight matrix of the armbands be $V = (0, \ldots, 0)_Q$, with the number of nearest neighbor samples being k(The exact value of k is determined by the cross-validation method, while also taking into consideration factors such as dataset size and feature size). We randomly select a sample R from D^* and find the k nearest neighbor samples H_j $(j = 1, 2, \ldots, k)$ of R from the same-class sample set. Find the k nearest neighbors M_j (C) $(j = 1, 2, \ldots, k)$ from each different-class sample set. The weight statistics of each channel are calculated using the following formula:

$$W(x) = W(x) - \sum_{j=1}^{k} diff(A, R, H_j) \Big/ (mk) + \sum_{C \neq Class(R)} \left[\frac{p(C) \times \sum_{j=1}^{k} diff(A, R, M_j(C))}{1 - p(Class(R))} \right] \Big/ (mk) \tag{3}$$

In the above formula, $p(C)$ represents the proportion of the channel, and $p(Class(R))$ represents the proportion of a randomly selected sample. $diff(R_1 - R_2)$ represents the difference between sample R_1 and R_2 on feature A, and M_j represents the j^{th} nearest neighbor sample in class C, as shown in the following formula:

$$diff(A, R_1, R_2) = \begin{cases} 0, & if\ A\ is\ discrete\ and\ R_1[x] = R_2[x] \\ \dfrac{|R_1[x] - R_2[x]|}{max(x) - min(x)}, & if\ A\ is\ continuous \\ 1, & if\ A\ is\ discrete\ and\ R_1[x] \neq R_2[x] \end{cases} \tag{4}$$

Repeat the above steps multiple times to update the statistical indicators of each channel, and record them in the weight matrix W of the channel in descending order. Calculate the canonical correlation coefficient ρ_Q for each of the Q armbands and the classification categories using the following formula:

$$\rho_{QM} = \frac{Cov(x, o)}{\sqrt{Var(x)}\sqrt{Var(o)}} \tag{5}$$

Let the total weight be $W(Q)$, and update the weight matrix of each channel as follows:

$$V(x) = \frac{W(x)}{W(Q)} + \frac{\rho_Q}{sum(\rho_Q)} \Big/ m \tag{6}$$

which represents the final channel weights obtained.

B. Channel Reduction

Correlation coefficients serve as pivotal metrics for quantifying the degree of association between variables, with Pearson, Spearman, and Kendall emerging as the three predominant measures in this domain. Notably, Spearman correlation [33], distinguished by its suitability for bivariate analyses, independence from several assumptions inherent to Pearson's correlation, and its applicability to ordinal data, finds particular utility in addressing issues involving nominal and ordinal data relationships.

In the present study, we adopt the Spearman correlation coefficient to investigate the interchannel relationships in a complex system. Specifically, we employ a hierarchical approach that involves selecting the most informative channels based on their importance ranking and iteratively removing the channels with high correlation values until a matrix is obtained that consists of only uncorrelated channel combinations. To be more precise, for a given set of channels, we compute the rho value and pval value for each pair of channels using the

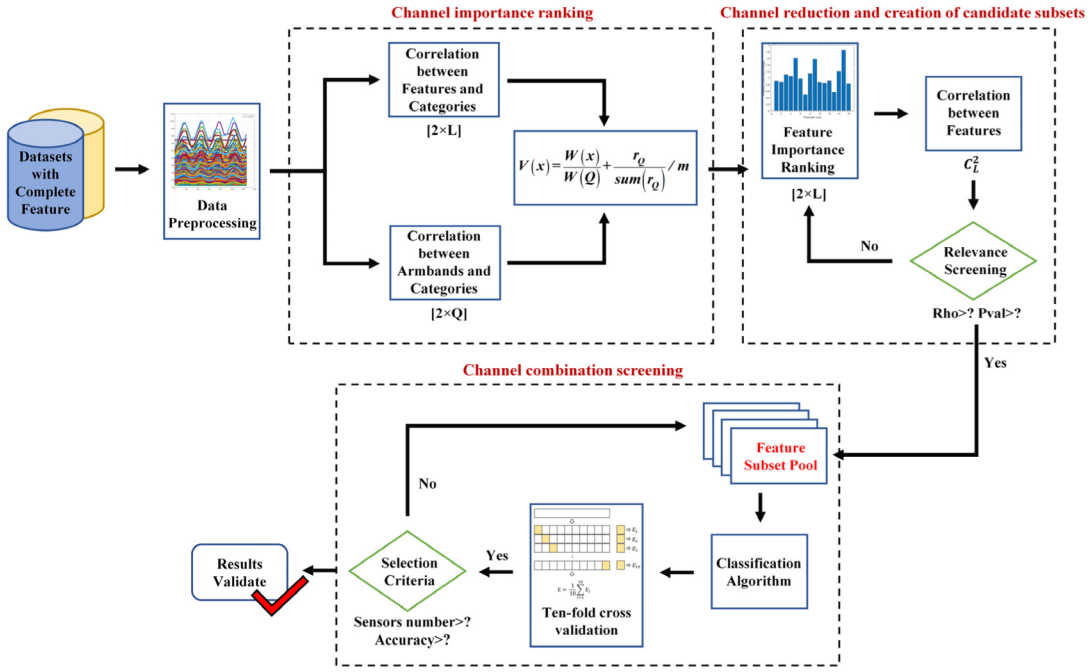

Fig. 2. Diagram of the channel selection algorithm.

Spearman correlation coefficient, its calculation formula is as follows:

$$rho\,(x, y) = 1 - \frac{6\sum d^2}{n\left(n^2 - 1\right)} \tag{7}$$

In this regard the variable d represents the difference between the ranks of two columns, while n denotes the length of each column. The Spearman rank correlation coefficient is represented by the rho value, and the corresponding p-value is denoted by pval. Channels with rho values exceeding 0.80 or pval values exceeding 0.05 are considered highly correlated and are removed from further analysis. This process is repeated iteratively until a matrix is obtained that consists of only uncorrelated channel combinations, where each row represents a unique combination of channels, and the correlation between any two combinations is less than 0.80.

C. Final Output

Prior research suggests that Linear Discriminant Analysis (LDA) excels in gesture classification [34]. Quadratic Discriminant Analysis (QDA), a variant of LDA, employs a similar implementation approach but employs distinct covariance matrices for each category, enhancing its flexibility. This study's data analysis demonstrates QDA's superior practical classification performance over LDA, leading to the selection of QDA as the classifier.

Once the channel combination matrix that has undergone correlation filtering is obtained, each combination (row) is sequentially input into the QDA classifier, and its classification accuracy is recorded and sorted based on accuracy. To avoid the limitations of fixed partitioning of the dataset and the problem of overfitting, ten-fold cross-validation is performed on each set of data. Finally, based on the user's input accuracy requirement, the channel combination with the fewest number of channels and the highest accuracy under the accuracy requirement is selected, and the corresponding combination and accuracy are output. If none of the combinations that rank first in accuracy meet the accuracy requirement, the first combination and its corresponding accuracy are directly outputted.

III. Materials and Methods

A. Participants

Fifteen participants were recruited [all males; age: 24.3 years (STD = 2.4); height: 174.7cm (STD = 4.7); weight: 67.7Kg (STD = 6.9); wrist circumference: 16.4cm (STD =0.7); forearm length: 24.7cm (STD = 0.9)], as shown in Table I. All participants were confirmed to be right-handed and possessed a healthy, unimpaired right arm and hand. They received adequate rest before the experiments to ensure no fatigue or stress during testing. Research assistants explained the procedure and purpose, obtaining written consent. Participants were assisted in placing arm straps on their right arms. They sat in standard chairs, following on-screen instructions for tasks. They were required to maintain stable posture to minimize external vibrations during data recording.

B. FMG Signal Acquisition System

We have designed an FMG signal acquisition system tailored for measuring the tendons and muscles responsible for finger movement and muscle activity. To meet experimental specifications, this apparatus is classified into two distinct types based on sensor quantity, and their respective internal configurations are illustrated in Fig. 5(a) and Fig. 5(b). This system consists of three FMG bands, four W504 signal amplification and filtering circuits, an STM32_F4VE microcontroller, a WCH CH340G Universal Serial Bus

Algorithm 1 The Optimal Channel Selection Algorithm

Input: Sample set $X = \{x_1, x_2, ..., x_N\}$, Sample set $Y = \{y_1, y_2, ..., y_M\}$, Accuracy requirement A, Number of nearest neighbours of the same type of sample $K = 90$

Output: Channel combination$\{C\}$, Accuracy rate *Accuracy*

$Sum \Leftarrow \emptyset$
for $m = 1 \rightarrow L$ **do** //L indicates the number of channels
  Calculate weight statistics for each channel by Eq.3
  for $i = 1 \rightarrow Q$ **do** //Q indicates the number of armbands
    Calculate the weight statistic for each armband by Eq.5
  end for
  Update the importance ranking of each channel by Eq.6
  WEIGHT(RANKED) = (X, Y)
end for
for $n = 2 \rightarrow L$ **do**
  for $i = 1 \rightarrow L$ **do**
    $Sum \Leftarrow$All results for the ranking combination C_L^n
    Calculate the values of rho and pval for the two channels in sum by Eq.8
    if $rho \geq 0.80$ or $pval \geq 0.05$ **then**
      Delete RANKED(i) from Sum
    end if
  end for
end for
Obtain a rich matrix of candidate subsets
for $Row(Sum) = 1 \rightarrow max$ **do**
  Calculate the classification accuracy of each group
  if $Accuracy \geq A$ **then**
    Output result with minimum number of channels
  else
    Output the first ranked result
  end if
end for
return C, *Accuracy*

Fig. 3. Channel selection algorithm pseudocode.

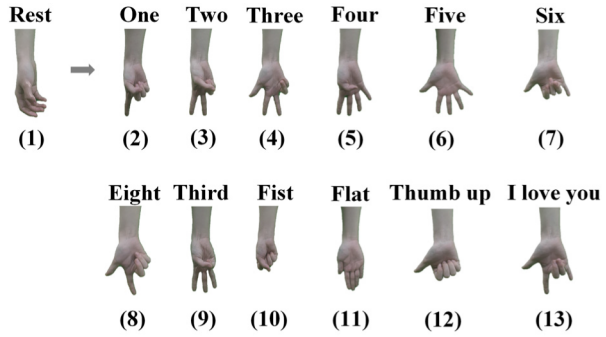

Fig. 4. A collection of 13 gestures selected from American Sign Language gestures needed to simulate daily life.

(USB) transmission module, and a personal computer. The Force-sensitive Resistor (FSR) used is a lightweight, small-sized, highly sensitive, and ultra-thin pressure-sensitive device (FSR, Interlink Electronics, Inc., Camarillo, CA, USA). Despite its reduced repeatability under high forces, it exhibits nearly linear behavior under low-force conditions. Among FSR sensor models, the FSR 402 with a relatively large contact area, chosen for FMG signal detection, is susceptible to bending during measurement. To ensure reliable sensor support, uniform force distribution, and freedom of movement on the elastic band, we enclosed the sensor with two 2.7 cm diameter thin sponges and attached a nylon strap to its back.

To enhance the flexibility of armband placement, we created three 28 cm long and 2.5 cm wide elastic bands. Sixteen sensors were evenly spaced at 3.5 centimeters intervals along each band, with four, six, and six sensors designated as F1, F2, and F3, respectively. These bands are longer than the participants' average forearm size, allowing for multiple parallel wrist or forearm placements to maximize sensor utilization during data collection. Each sensor was connected to signal amplification and filtering circuits and processed using the STM32_F4VE microcontroller's embedded 12-bit resolution A/D converter. Finally, the system connected to a standard laptop through a built-in USB interface for further processing and analysis.

This study also developed a Graphical User Interface (GUI) using Python for real-time FMG signal data collection. The GUI provides real-time data information for each channel and allows participants to perform gesture actions according to instructions. The operator can manually select when to start, pause, and save data. Before each data collection, a 5-second countdown prepares the participant. Upon completion, the data is automatically saved in CSV format and the panel is updated to display the next gesture.

TABLE I
PHYSICAL DATA OF ALL PARTICIPANTS

Participants	age	Height (cm)	Weight (kg)	wrist circumference (cm)	forearm length (cm)
S1	26	175	70	17	24
S2	23	173	65	16	23
S3	23	187	65	16	25.5
S4	22	175	74	15.5	26
S5	22	180	82	16.5	25.5
S6	22	173	58	15	25.5
S7	25	168	77	18	24
S8	26	170	58	16	24
S9	24	170	72	18	24
S10	30	181	72	16	25.5
S11	25	171	60	16	24
S12	25	176	64	16	24
S13	26	175	70	17	24
S14	23	173	68	16	23
S15	22	173	60	15	25.5
Average	**24.3**	**174.7**	**67.7**	**16.3**	**24.5**

C. Gesture Set and Experimental Design

In this study, offline FMG data was collected from 15 participants under various wearing conditions that simulated typical real-life usage scenarios using our equipment. The gesture set includes 13 hand gestures selected from American Sign Language (ASL), as shown in Fig. 4, which are often used in daily life rehabilitation training. The experiment was divided into two groups, with 10 participants in the first group using 16 sensors to collect gesture data. Fig. 5(d) displays

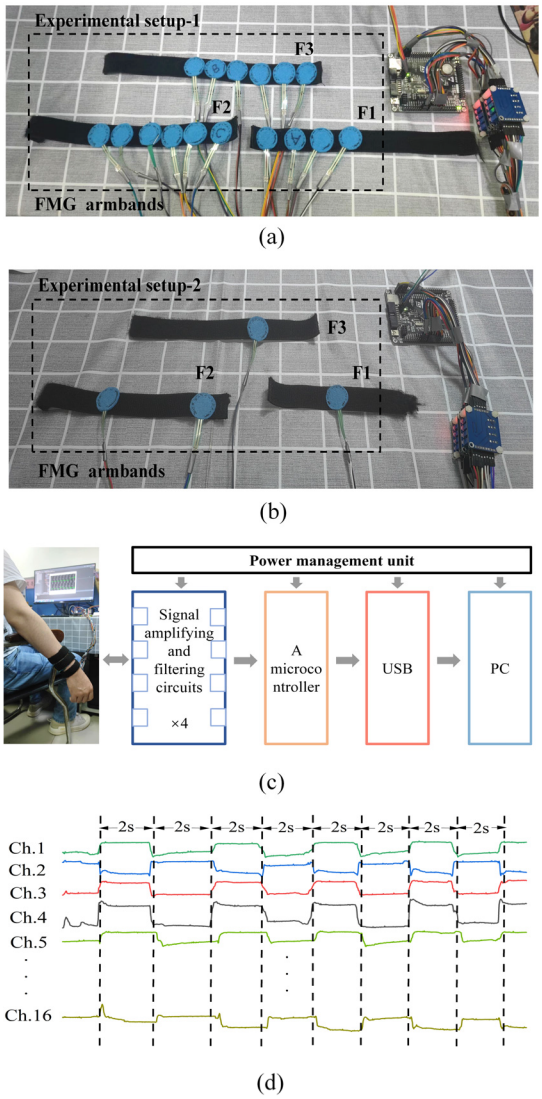

Fig. 5. (a) Experimental setup one is a three armbands FMG signal acquisition system containing 16 wrapped FSR 402 sensors. (b) Experimental setup two is a three armbands FMG signal acquisition system containing four wrapped FSR 402 sensor. (c) Block diagram of the main hardware structure that makes up the FMG signal acquisition system. (d) Example of a raw waveform recorded from all 16 channels in a gesture action.

an example waveform of all 16 channels recorded during the measurement of a certain gesture action. After analyzing and organizing the collected data to obtain a universal measuring point combination, the remaining 5 untested participants were used to verify the experiment. The experimental protocol was approved by the Ethics Committee of Huazhong University of Science and Technology.

Before conducting the experiments, participants underwent a washing procedure on their right arm followed by complete drying to prevent measurement data errors caused by dirt. The three armbands were then placed in proximity to the wrist, with each band (F1, F2, and F3) being sequentially positioned towards the arm. The armband F1, which was equipped with four-channel sensors, was positioned nearest to the wrist. The first sensor of each armband was roughly aligned with the styloid process of the ulna, while the other sensors were evenly

TABLE II
ACCURACY OF PARTICIPANTS AFTER DIFFERENT CHANNEL SELECTION

Participants	Accuracy(%)↑				
	Ours	Relief-F	ILFS	CFS	mRMR
S1	**93.73**	86.70	92.40	90.10	92.70
S2	90.64	81.10	83.70	86.10	**91.80**
S3	95.12	90.50	91.50	92.40	**96.00**
S4	**95.65**	84.80	88.40	93.50	89.30
S5	**95.90**	64.30	66.10	68.50	95.86
S6	**96.87**	93.0	89.90	71.70	96.50
S7	**96.45**	78.30	87.10	87.50	82.10
S8	93.30	91.80	91.90	**94.10**	90.40
S9	**94.53**	90.0	93.20	91.10	93.30
S10	91.93	84.10	87.00	90.20	**93.50**
Average↑	**94.41**	84.46	87.12	86.52	92.14

spaced around the arm. The distance between the upper edge of F1 and the styloid process of the ulna at the right wrist was 2 cm, and the distance between the upper edges of F1, F2, and F3 was 3 cm, thereby creating three parallel rings.

Each participant was instructed to perform the 13 gestures according to the instructions provided in the GUI. The sampling frequency of the acquisition system was set to 70Hz. To avoid the influence of the start and end buttons on the data, the recording time of each measurement was slightly longer than 20 seconds. During a single data recording process, participants had 5 seconds to transition, 2 seconds to maintain the gesture, 2 seconds to relax and return to a static state, and 2 seconds to maintain the gesture again, alternating back and forth. To avoid fatigue, participants rested for 10 seconds between each pair of gestures, and each gesture was measured twice. The data collected during this period was arranged into a matrix, with each row corresponding to the data of each sensor, and the data was saved in a CSV file.

The FMG signal data collected during the experiment was processed offline using MATLAB software by MathWorks. Continuous measurements were taken from participants while they performed each action, yielding data without significant fluctuations, thus negating the necessity for intricate feature extraction. A sliding average filter was initially applied to the raw FMG signal samples to mitigate noise arising from instruments and the environment. As recommended in [12] and [35], a window length of 200 ms and a moving step size of 50 ms were employed for sliding filtering, aligning with the suggested range of 150-250 ms. Given the relatively concentrated values and to neutralize the impact of individual sample data, the filtered data underwent normalization using the min-max normalization method.

IV. RESULTS AND DISCUSSION

A. Results of Channel Selection

Table II displays the results of ten participants who utilized the proposed channel selection algorithm. The comparison is

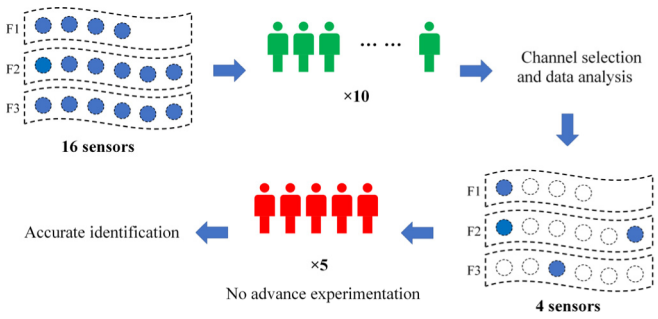

Fig. 6. Overall experimental flow diagram.

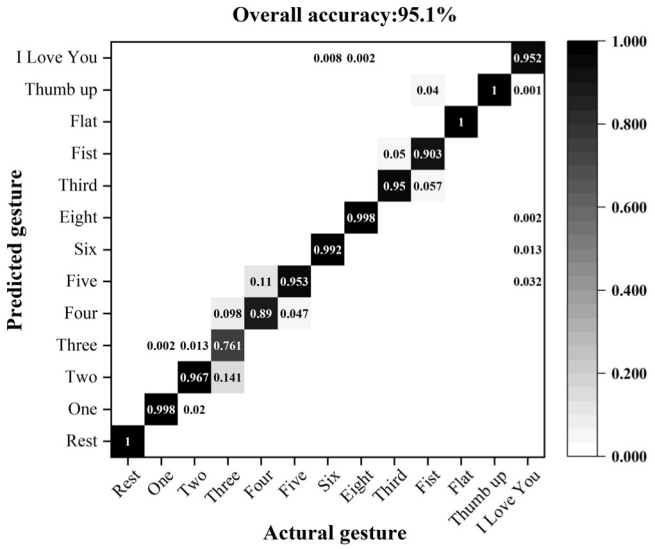

Fig. 7. Confusion matrix of the classification of a standard participant whose stature meets the WTO criteria.

made to four benchmark algorithms to identify the optimal channel combination. The results indicate that four channels were the most commonly selected by the participants, with recognition accuracies ranging from 90.64% to 96.87%. The average number of channels selected by the participants was four, which is equivalent to an 75% reduction in the original number of channels. This finding demonstrates the effectiveness of the proposed channel selection algorithm in eliminating redundant channels. We obtain a satisfactory average recognition accuracy of 94.46%. Fig. 7 displays the classification confusion matrix to illustrate the prediction performance of a male participant who met the body size and health standards set by the World Health Organization (WHO), i.e., a height of 175 cm and BMI of 22.9. We observe that the "Three" gesture had the worst prediction performance for the standard individual, with a 76.2% classification accuracy. This implies that the muscles used in the "Three" gesture are similar to those utilized in the "Four" and "Two" gestures.

Relief-F, Max-Relevance Min-Redundancy (mRMR), Correlation-based Feature Selection (CFS), and ILFS are four commonly used and highly effective feature selection algorithms in the field of gesture recognition.

Relief-F [36] assigns weights to variables based on their ability to distinguish nearby data points in binary classification. mRMR attempts to find a subset of variables with high correlations with the target variable, while also having low mutual correlation between variables. Similarly, CFS [37] algorithm is based on the assumption that a good subset of features should contain highly correlated features with the target, while being unrelated to each other. ILFS [38], [39], a 2017 algorithm, excels by considering all possible feature subsets, thus bypassing combinatorial issues, and outperforming advanced selection methods. Since all three feature selection algorithms, Relief-F, mRMR, and ILFS, only perform importance ranking without a specified stopping criterion, the ranking of the entire 16 channels will be obtained after data processing. To address this, we initially apply our proposed channel selection algorithm to the data of ten participants, obtaining a reduced feature set and corresponding accuracy assessment. Subsequently, we proceed to sequentially extract the top n features from the Relief-F, mRMR, and ILFS methods, ensuring a consistent number of features as selected in the previous step. Furthermore, for the CFS algorithm, we establish a maximum feature count equivalent to the number of channels selected. The search process is halted either when the identified feature subset reaches this predetermined count or when consecutive iterations fail to yield a superior feature subset. Perform QDA classification on the selected feature sets from each method and record the accuracy.

The classification results from the ten participants are compared for the five methods, with results better than ours being emphasized in Table II. Our method produces superior performance over Relief-F and ILFS. However, for the mRMR method, three participants had slightly lower results than mRMR (1.20%±0.28), and for the CFS method, one participant had a slightly lower result than CFS (0.8%). Since the ten-fold cross-validation in QDA has inherent randomness, the classification accuracy can vary slightly depending on the grouping, and the difference in accuracy is only about 1% compared to the other results. Therefore, it can be considered that our method is equivalent to the other two on these four participants. Observing the average recognition accuracy of the ten participants for each method, it can be seen that our method outperformed the other four methods, with a recognition accuracy of 94.41%. Thus, our method for selecting the optimal combination of measurement points and outputting its accuracy in gesture recognition has demonstrated superiority.

B. Location and Validation of the General Sensors Combination

Due to variations in measurement point positions, which can result in different muscle change data, the accuracy and stability of measurement point placement have a significant impact on experimental outcomes [40]. To provide a universal set of measurement points, the number of times each of the 16 channels appeared in all channel combinations selected by ten participants was recorded. The more times a channel appeared, the more important it was. To facilitate subsequent modeling, a two-dimensional coordinate system was established with the back of the hand facing upward, the styloid process of the ulna on the right forearm as the origin, the direction perpendicular to the wrist as the x-axis and the direction along the arm as

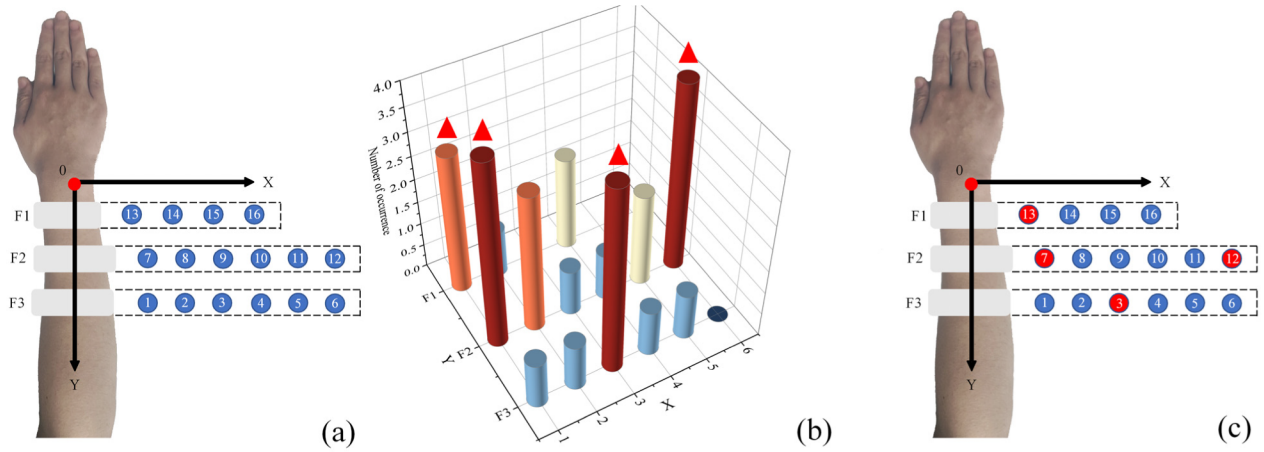

Fig. 8. Ten participants performed 13 gesture recognition experiments with results obtained after channel selection. (a) Schematic diagram of the placement of three armbands and 16 sensors used in the experiments. A plane rectangular coordinate system was established with the styloid process of the ulna as the origin, the y-axis along the arm and the x-axis perpendicular to the arm. (b) Statistics on the number of occurrences of channels selected after channel selection for ten participants. The x-axis and y-axis in the figure correspond to the X and Y directions of the rectangular coordinate system, respectively. Each cylinder corresponds to a channel in Figure (a). The higher the cylinder, the more frequently the channel occurs. (c) Optimal position of the selected channel in the armbands.

the y-axis, as show in Fig. 8(a). The number of times each channel appeared was recorded as shown in the Fig. 8(b). F1, F2, and F3 represent three armbands, and F1-1, F2-1, and F3-1 represent the first points on each armband, all on the y-axis, with the remaining measurement points arranged equidistantly on each arm strap. From the Fig. 8(b), it can be seen that the measurement points F2-1, F2-6, and F3-3 appeared the most frequently and equally among all measurement points, with a total of four times each. To ensure the completeness of the selected channel combinations, the point F1-1 with the highest frequency of appearance on strap F1 was added. The final universal measurement point combination selecte include F1-1, F2-1, F2-6, and F3-3. The position in the armbands is shown in Fig. 8(c).

The actual position of the same measurement point may vary due to many exterior factor. To improve the precision of the position of the universal measurement points combination, the four universal measurement points of ten participants were mapped and standardized onto a planar Cartesian coordinate system. This was achieved by dividing the x value of the actual measurement position of each point by the circumference of the participant's wrist and dividing the y value by the length of the participant's forearm. Fig. 9 illustrates the position of all mapped points of the ten participants in the coordinate system. By computing the minimum covering circle of the position of the four points, the x and y coordinates of the circle center represent the recommended universal measurement points in the upper arm coordinate system.

Table IV presents the coordinate positions of the selected universal measurement points after mapping. Consequently, the normalized positions and coverage size (X_n, Y_n, R_n) of the universal measurement points combination comprising the four points are computed as (0.408, 0.364, 0.065), (0, 0.240, 0.001), (0.906, 0.248, 0.034), and (0, 0.128, 0.003). Fig. 10 depicts the position of the universal measurement points combination on the upper arm of the human body. To use this system, the experimenter first measures the wrist circumference and forearm length of the participant, then multiplies them by the corresponding x and y values of the four points to obtain the position of the points on the participant's upper arm.

To validate the results of the universal measuring points, we use five participants who had not undergone prior experiments. The experimenter measured the wrist circumference and forearm length of each participant, and then multiplied the x and y values of the four universal measuring points by the respective participant's body values to calculate the positions of the four points. The four sensors were then placed on the corresponding positions on the participants' arms for the 13-gesture recognition experiment, with data collection and processing procedures similar to previous experiments. The results, as shown in Table III, indicate that using only four measuring points, the recognition accuracy for the five participants reached 96.5%, 94.2%, 96.8%, 95.7%, and 98.2%, respectively. This demonstrates that the universal measuring point coordinates exhibit strong robustness and recognition performance in actual gesture recognition tasks.

V. Limitations and Future Work

While our investigation has yielded encouraging outcomes in the advancement of intelligent channel selection methodologies for gesture recognition, several hurdles merit attention for future inquiry.

1) **Limitations of FMG Signals:** Firstly, the acquisition of FMG signals is susceptible to the influence of muscle movements, which may result in decreased signal quality or distortion due to muscle fatigue or movement instability. Additionally, physiological and environmental factors can also impact FMG, such as sweat and dirt, which may reduce the quality of sensor-to-skin contact, thereby affecting the accuracy and quality of FMG signals. During signal transmission and processing, delays and instabilities may exist, particularly in scenarios requiring rapid responses, potentially affecting real-time performance and accuracy. Furthermore, the

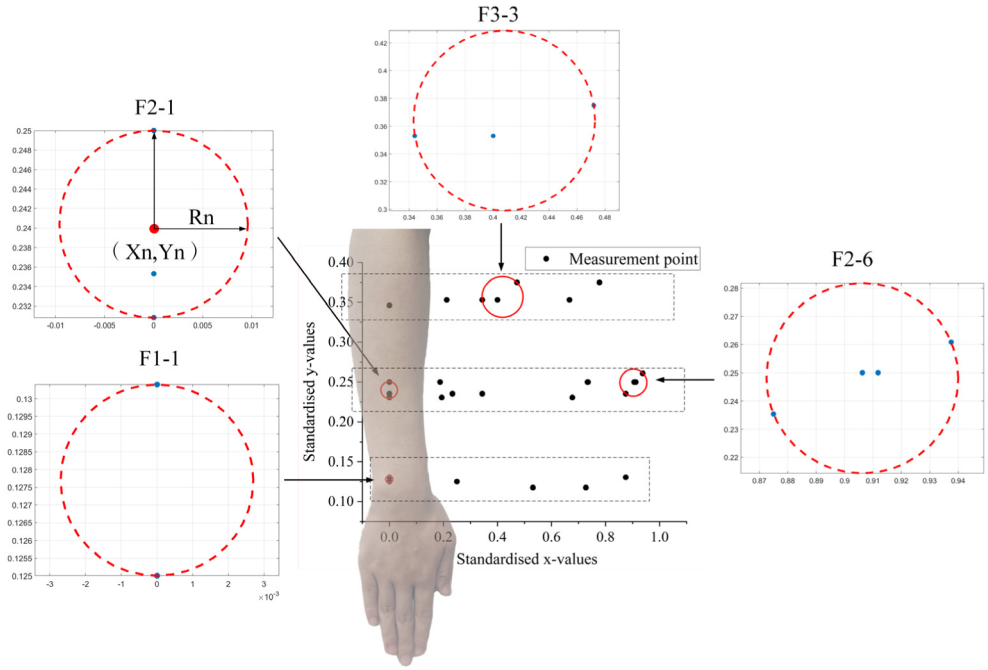

Fig. 9. Optimal channel positions selected by the 10 participants plotted on the plane rectangular coordinate system. Using F1-1, F2-1, F2-6, and F3-3 as the universal channel combination, the minimum coverage circles for all positions of these four points were calculated and magnified, with the coordinates of the circle centers representing the optimal channel positions.

TABLE III
DATA FROM PARTICIPANTS WHO VALIDATED THE OPTIMAL COMBINATION OF MEASUREMENT POINTS

Participants	Forearm length (cm)	Wrist circumference (cm)	Position				Accuracy (%)
			1	2	3	4	
1	24	16	(6.53, 8.73)	(0, 5.77)	(14.50, 5.95)	(0, 3.06)	96.5
2	24	16	(6.53, 8.73)	(0, 5.77)	(14.50, 5.95)	(0, 3.06)	94.2
3	24	17	(6.94, 8.73)	(0, 5.77)	(15.41, 5.95)	(0, 3.06)	96.8
4	23	16	(6.53, 8.37)	(0, 5.53)	(14.50, 5.70)	(0, 2.94)	95.7
5	25.5	15	(6.12, 9.28)	(0, 6.13)	(16.59, 6.32)	(0, 3.26)	98.2

TABLE IV
COORDINATES OF THE OPTIMAL COMBINATION OF MEASUREMENT POINTS

	X_n	Y_n	R_n
F1-1	0	0.1277	0.0027
F2-1	0	0.2404	0.0096
F2-6	0.9062	0.2480	0.0338
F3-3	0.4080	0.3639	0.0652

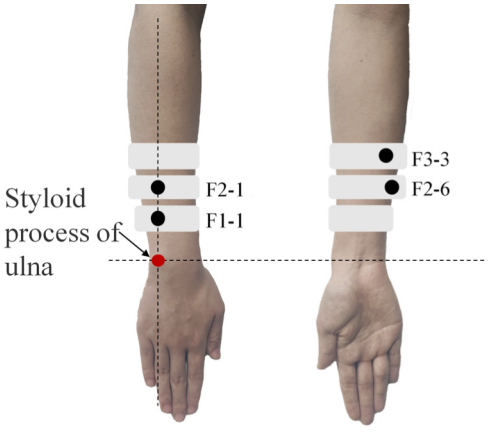

Fig. 10. The location of the universal channel combination on the arm is provided, with the red dot indicating the styloid process of the ulna.

sensitivity of FMG signals is limited, especially in cases of weak or inconspicuous muscle contractions, making signal extraction challenging and increasing data uncertainty. Additionally, the analysis and processing of FMG signals face challenges such as noise removal, feature extraction, and classification algorithm design. Therefore, when applying FMG to gesture recognition systems, it is necessary to comprehensively consider these limitations and take corresponding measures to overcome them, ensuring system performance and reliability.

2) **Participant Diversity:** Notably, our study was confined to a cohort comprising solely 15 healthy male individuals, thereby potentially limiting the representativeness of our findings to the broader populace. Therefore, it is imperative to encompass a more heterogeneous participant pool, encompassing individuals across diverse genders, age groups, and health statuses, to bolster the accuracy and applicability of the proposed methodology.
3) **Customized Arm Band Development and Disability Applications:** The development of tailored arm bands predicated on optimal sensor positioning, coupled with the deployment of gesture recognition technology in individuals afflicted with upper limb disabilities, represent promising avenues for future research endeavors. Such applications hold the potential to markedly enhance the usability and accessibility of gesture recognition systems across diverse domains.

In summation, the resolution of these challenges will be pivotal for the progression and practical deployment of our proposed intelligent channel selection methodology within gesture recognition frameworks.

VI. Conclusion

In this investigation, we propose a novel approach to channel selection, enabling users to determine the optimal number and location of sensors for gesture recognition through data collected from a high-density FMG system. This approach facilitates the design of customized devices that cater to individual needs. Additionally, a universal model for sensor placement is established based on upper limb muscle change data obtained from ten participants and validated on other five subjects. Our approach takes into account the distribution of armbands and sensors in specific experiments, the assignment of sensor weight coefficients, which greatly enriching the subset of candidates and effectively avoiding falling into local optima.

Acknowledgment

The authors would like to thank Zihao Du, Denan Xu, and Hao Wang for their assistance during the experimental measurements.

References

[1] H. Shahsavari et al., "Upper limb amputation; care needs for reintegration to life: An integrative review," *Int. J. Orthopaedic Trauma Nursing*, vol. 38, Aug. 2020, Art. no. 100773, doi: 10.1016/j.ijotn.2020.100773.
[2] G. Buodo, C. Novara, M. Ghisi, and D. Palomba, "Posttraumatic and depressive symptoms in victims of occupational accidents," *Depression Res. Treat.*, vol. 2012, May 2012, Art. no. 184572, doi: 10.1155/2012/184572.
[3] X. Wang, H. Yu, S. Kold, O. Rahbek, and S. Bai, "Wearable sensors for activity monitoring and motion control: A review," *Biomimetic Intell. Robot.*, vol. 3, no. 1, Mar. 2023, Art. no. 100089, doi: 10.1016/j.birob.2023.100089.
[4] I. Boukhennoufa, X. Zhai, V. Utti, J. Jackson, and K. D. McDonald-Maier, "Wearable sensors and machine learning in post-stroke rehabilitation assessment: A systematic review," *Biomed. Signal Process. Control*, vol. 71, Jan. 2022, Art. no. 103197, doi: 10.1016/j.bspc.2021.103197.
[5] V. I. Pavlovic, R. Sharma, and T. S. Huang, "Visual interpretation of hand gestures for human-computer interaction: A review," *IEEE Trans. Pattern Anal. Mach. Intell.*, vol. 19, no. 7, pp. 677–695, Jul. 1997, doi: 10.1109/34.598226.
[6] C. Castellini and R. Koiva, "Using a high spatial resolution tactile sensor for intention detection," in *Proc. IEEE 13th Int. Conf. Rehabil. Robot. (ICORR)*, Jun. 2013, pp. 1–7, doi: 10.1109/ICORR.2013.6650365.
[7] A. Y. Karatayev, L. E. Burlakova, T. D. Miller, and M. F. Perrelli, "Reconstructing historical range and population size of an endangered mollusc: Long-term decline of popenaias popeii in the rio grande, Texas," *Hydrobiologia*, vol. 810, no. 1, pp. 333–349, Mar. 2018, doi: 10.1007/s10750-015-2551-3.
[8] C. Castellini, E. Gruppioni, A. Davalli, and G. Sandini, "Fine detection of grasp force and posture by amputees via surface electromyography," *J. Physiol.-Paris*, vol. 103, nos. 3–5, pp. 255–262, 2009, doi: 10.1016/j.jphysparis.2009.08.008.
[9] K. Li, J. Zhang, L. Wang, M. Zhang, J. Li, and S. Bao, "A review of the key technologies for sEMG-based human–robot interaction systems," *Biomed. Signal Process. Control*, vol. 62, Sep. 2020, Art. no. 102074, doi: 10.1016/j.bspc.2020.102074.
[10] L. Schreiner, S. Sieghartsleitner, K. Mayr, H. Pretl, and C. Guger, "Hand gesture decoding using ultra-high-density EEG," in *Proc. 11th Int. IEEE/EMBS Conf. Neural Eng. (NER)*, Apr. 2023, pp. 01–04, doi: 10.1109/NER52421.2023.10123901.
[11] M.-K. Liu, Y.-T. Lin, Z.-W. Qiu, C.-K. Kuo, and C.-K. Wu, "Hand gesture recognition by a MMG-based wearable device," *IEEE Sensors J.*, vol. 20, no. 24, pp. 14703–14712, Dec. 2020, doi: 10.1109/JSEN.2020.3011825.
[12] Y. Fang, N. Hettiarachchi, D. Zhou, and H. Liu, "Multi-modal sensing techniques for interfacing hand prostheses: A review," *IEEE Sensors J.*, vol. 15, no. 11, pp. 6065–6076, Nov. 2015, doi: 10.1109/JSEN.2015.2450211.
[13] H. Fang et al., "Anatomically designed triboelectric wristbands with adaptive accelerated learning for human–machine interfaces," *Adv. Sci.*, vol. 10, no. 6, 2023, Art. no. 2205960, doi: 10.1002/advs.202205960.
[14] O. Sherif, M. M. Bassuoni, and O. Mehrez, "A survey on the state of the art of force myography technique (FMG): Analysis and assessment," *Med. Biol. Eng. Comput.*, vol. 62, no. 5, pp. 1313–1332, May 2024, doi: 10.1007/s11517-024-03019-w.
[15] W. Guo, Y. Fang, X. Sheng, and X. Zhu, "Measuring motor unit discharge, myofiber vibration, and haemodynamics for enhanced myoelectric gesture recognition," *IEEE Trans. Instrum. Meas.*, vol. 72, pp. 1–10, 2023, doi: 10.1109/TIM.2023.3234092.
[16] E. Nsugbe, "Brain-machine and muscle-machine bio-sensing methods for gesture intent acquisition in upper-limb prosthesis control: A review," *J. Med. Eng. Technol.*, vol. 45, no. 2, pp. 115–128, Feb. 2021, doi: 10.1080/03091902.2020.1854357.
[17] X. Jiang, L.-K. Merhi, and C. Menon, "Force exertion affects grasp classification using force myography," *IEEE Trans. Human-Mach. Syst.*, vol. 48, no. 2, pp. 219–226, Apr. 2018, doi: 10.1109/THMS.2017.2693245.
[18] A. Dementyev and J. A. Paradiso, "WristFlex: low-power gesture input with wrist-Worn pressure sensors," in *Proc. 27th Annu. ACM symposium User Interface Softw. Technol.*, 2014, pp. 161–166, doi: 10.1145/2642918.2647396.
[19] X. Jiang, L.-K. Merhi, Z. G. Xiao, and C. Menon, "Exploration of force myography and surface electromyography in hand gesture classification," *Med. Eng. Phys.*, vol. 41, pp. 63–73, Mar. 2017, doi: 10.1016/j.medengphy.2017.01.015.
[20] A. Belbasis and F. K. Fuss, "Muscle performance investigated with a novel smart compression garment based on pressure sensor force myography and its validation against EMG," *Frontiers Physiol.*, vol. 9, pp. 1–13, Apr. 2018, doi: 10.3389/fphys.2018.00408.
[21] A. Prakash, A. K. Sahi, N. Sharma, and S. Sharma, "Force myography controlled multifunctional hand prosthesis for upper-limb amputees," *Biomed. Signal Process. Control*, vol. 62, Sep. 2020, Art. no. 102122, doi: 10.1016/j.bspc.2020.102122.
[22] N. Li, D. Yang, L. Jiang, H. Liu, and H. Cai, "Combined use of FSR sensor array and SVM classifier for finger motion recognition based on pressure distribution map," *J. Bionic Eng.*, vol. 9, no. 1, pp. 39–47, Mar. 2012, doi: 10.1016/s1672-6529(11)60095-4.
[23] M. J. Cheok, Z. Omar, and M. H. Jaward, "A review of hand gesture and sign language recognition techniques," *Int. J. Mach. Learn. Cybern.*, vol. 10, no. 1, pp. 131–153, Jan. 2019, doi: 10.1007/s13042-017-0705-5.
[24] V. M. Gulhane and D. A. Kumbhare, "Biomedical applications using hand gesture with electromyography control signal," *Comput. Intell. Mach. Learn.*, vol. 3, no. 2, pp. 31–38, Oct. 2022, doi: 10.36647/ciml/03.02.a005.

[25] Z. G. Xiao and C. Menon, "A review of force myography research and development," *Sensors*, vol. 19, no. 20, p. 4557, Oct. 2019, doi: 10.3390/s19204557.

[26] D. Ferigo, L.-K. Merhi, B. Pousett, Z. G. Xiao, and C. Menon, "A case study of a force-myography controlled bionic hand mitigating limb position effect," *J. Bionic Eng.*, vol. 14, no. 4, pp. 692–705, Dec. 2017.

[27] A. Radmand, E. Scheme, and K. Englehart, "High-density force myography: A possible alternative for upper-limb prosthetic control," *J. Rehabil. Res. Develop.*, vol. 53, no. 4, pp. 443–456, 2016, doi: 10.1682/jrrd.2015.03.0041.

[28] M. Sakr and C. Menon, "Study on the force myography sensors placement for robust hand force estimation," in *Proc. IEEE Int. Conf. Syst., Man, Cybern. (SMC)*, Oct. 2017, pp. 1387–1392, doi: 10.1109/SMC.2017.8122807.

[29] G. Lei, S. Zhang, Y. Fang, Y. Wang, and X. Zhang, "Investigation on the sampling frequency and channel number for force myography based hand gesture recognition," *Sensors*, vol. 21, no. 11, p. 3872, Jun. 2021, doi: 10.3390/s21113872.

[30] G. Chandrashekar and F. Sahin, "A survey on feature selection methods," *Comput. Electr. Eng.*, vol. 40, no. 1, pp. 16–28, Jan. 2014, doi: 10.1016/j.compeleceng.2013.11.024.

[31] U. M. Khaire and R. Dhanalakshmi, "Stability of feature selection algorithm: A review," *J. King Saud Univ.-Comput. Inf. Sci.*, vol. 34, no. 4, pp. 1060–1073, Apr. 2022, doi: 10.1016/j.jksuci.2019.06.012.

[32] C. Ahmadizadeh, B. Pousett, and C. Menon, "Investigation of channel selection for gesture classification for prosthesis control using force myography: A case study," *Frontiers Bioeng. Biotechnol.*, vol. 7, pp. 1–15, Dec. 2019, doi: 10.3389/fbioe.2019.00331.

[33] Z. Wang, Y. Fang, G. Li, and H. Liu, "Facilitate sEMG-based human–machine interaction through channel optimization," *Int. J. Humanoid Robot.*, vol. 16, no. 4, pp. 1–19, 2019, doi: 10.1142/S0219843619410019.

[34] K. Ali and A. Al-Hameed, "Spearman's correlation coefficient in statistical analysis," *Int. J. Nonlinear Anal. Appl.*, vol. 13, no. May 2021, pp. 2008–6822, 2022, doi: 10.22075/ijnaa.2022.6079.

[35] A. H. Al-Timemy, Y. Serrestou, R. N. Khushaba, S. Yacoub, and K. Raoof, "Hand gesture recognition with acoustic myography and wavelet scattering transform," *IEEE Access*, vol. 10, pp. 107526–107535, 2022, doi: 10.1109/ACCESS.2022.3212146.

[36] L. H. Smith, L. J. Hargrove, B. A. Lock, and T. A. Kuiken, "Determining the optimal window length for pattern recognition-based myoelectric control: Balancing the competing effects of classification error and controller delay," *IEEE Trans. Neural Syst. Rehabil. Eng.*, vol. 19, no. 2, pp. 186–192, Apr. 2011, doi: 10.1109/TNSRE.2010.2100828.

[37] X. Jiang et al., "Optimization of HD-sEMG-Based cross-day hand gesture classification by optimal feature extraction and data augmentation," *IEEE Trans. Human-Mach. Syst.*, vol. 52, no. 6, pp. 1281–1291, Dec. 2022, doi: 10.1109/THMS.2022.3175408.

[38] A. Pavlidou et al., "Hand gesture performance is impaired in major depressive disorder: A matter of working memory performance?" *J. Affect. Disorders*, vol. 292, pp. 81–88, Sep. 2021, doi: 10.1016/j.jad.2021.05.055.

[39] G. Roffo, S. Melzi, U. Castellani, and A. Vinciarelli, "Infinite latent feature selection: A probabilistic latent graph-based ranking approach," in *Proc. IEEE Int. Conf. Comput. Vis.*, Oct. 2017, pp. 1407–1415, doi: 10.1109/ICCV.2017.156.

[40] F. Xiao, D. Yang, Z. Lv, X. Guo, Z. Liu, and Y. Wang, "Classification of hand movements using variational mode decomposition and composite permutation entropy index with surface electromyogram signals," *Future Gener. Comput. Syst.*, vol. 110, pp. 1023–1036, Sep. 2020, doi: 10.1016/j.future.2019.11.025.

[41] L. Meng et al., "User-tailored hand gesture recognition system for wearable prosthesis and armband based on surface electromyogram," *IEEE Trans. Instrum. Meas.*, vol. 71, pp. 1–16, 2022, doi: 10.1109/TIM.2022.3217868.